Application of Acoustic Signals for Rectifier Fault Detection in Brushless Synchronous Generator

Mehdi RAHNAMA, Abolfazl VAHEDI*

Department of Electrical Engineering
Center of Excellence for Power System Automation and Operation
Iran University of Science and Technology (IUST)
Narmak 16846, Tehran, Iran
*Corresponding Author e-mail: avahedi@iust.ac.ir

One of the most important issues that power companies face when trying to reduce time and cost maintenance is condition monitoring. In electricity market worldwide, a significant amount of electrical energy is produced by synchronous machines. One type of these machines is brushless synchronous generators in which the rectifier bridge is mounted on rotating shafts. Since bridge terminals are not accessible in this type of generators, it is difficult to detect the possible faults on the rectifier bridge. Therefore, in this paper, a method is proposed to facilitate the rectifier fault detection. The proposed method is then evaluated by applying two conventional kinds of faults on rectifier bridges including one diode open-circuit and two diode open-circuit (one phase open-circuit of the armature winding in the auxiliary generator in experimental set). To extract suitable features for fault detection, the wavelet transform has been used on recorded audio signals. For classifying faulty and healthy states, K-Nearest Neighbours (KNN) supervised classification method was used. The results show a good accuracy of the proposed method.

Keywords: acoustic emission; wavelet transform; K-Nearest Neighbours; fault detection; brushless generator.

1. Introduction

The electricity grid is the largest human-made network in which synchronous generator is one of the most important equipment pieces of power plants that is responsible for converting mechanical energy to electrical one. The basis of electricity generation is the electromagnetic induction. Online fault detection is important since the development of defect and increasing the cost and repair time is prevented. The importance of this issue has increased even more due to the privatisation of the power industry and the presence of power plants in the electricity market. Therefore, condition monitoring and accurate fault detection in the minimum time are considerably significant. One type of the synchronous generator is the brushless synchronous generator in which a rectifier bridge is used to provide a direct current for producing a magnetic field. Since the rectifier is located on the shaft of the generator, it is not directly accessible. Therefore, to detect possible occurring faults on the rectifier, a fault detection

method must be considered in which the fault can be detected without any electrical contact with the rectifier.

Some of the used methods for detecting the faults are vibration analysis (HU *et al.*, 2017; SINGH, PAREY, 2017; WANG *et al.*, 2017; Narendiranath Babu T. *et al.*, 2018; PRAVEENKUMAR *et al.*, 2018; ZHANG *et al.*, 2018), current analysis (SHAH, BHALJA, 2016; REZAZADEH MEHRJOU *et al.*, 2017; HAROUN *et al.*, 2018), and sound wave analysis (CHACON *et al.*, 2015; GLOWACZ, 2015; 2016; 2018; GLOWACZ, GLOWACZ, 2017a; 2017b; GLOWACZ *et al.*, 2018; VAIMANN *et al.*, 2018). Due to the fact that the fault detection method based on the audio signal reveals faults faster than other common methods (CHACON *et al.*, 2015), this technique is used for fault detection. Therefore, fault detection by acoustic signals has been investigated for many applications. In (CHACON *et al.*, 2015) bearing defects detection of rotary machines using the acoustic signal in different signal-to-noise ratio conditions has been investigated based on

wavelet packet transform. In (Glowacz, 2015), using Fast Fourier Transformation, Method of Selection of Amplitudes of Frequencies (MSAF-5), and Linear Support Vector Machine classifier, the recognition of acoustic signals of a loaded synchronous motor is investigated for different states including healthy loaded synchronous motor, loaded synchronous motor with shorted stator coil, loaded synchronous motor with shorted stator coil and broken coil, loaded synchronous motor with shorted stator coil and two broken coils. In (Glowacz, 2016), a feature extraction method, shortened method of frequencies selection-25-Expanded, is utilised for fault detection of loaded synchronous motor based on acoustic signals. Sound signal analysis is also utilised for short-circuit fault analysis in the main winding and auxiliary coil of single-phase induction motor using KNN classifier (Glowacz, Glowacz, 2017a). Using a feature extraction method called the shortened method of frequencies selection for acoustic signals of a DC motor, a fault detection approach is proposed in (Glowacz, Glowacz, 2017b). Five states of the commutator motor are considered for fault detection of the motor in (Glowacz, 2018) where some classification methods, such as nearest mean, nearest neighbour, back propagation neural network, and self-organising map are used for acoustic analysis. In addition, three states of an induction motor including healthy state, faulty bearing, and faulty bearing and shortened coils of auxiliary winding are measured and analysed for fault detection of the motor using the nearest neighbour, nearest mean, and Gaussian mixture models as classifiers in (Glowacz *et al.*, 2018). A fault detection approach is proposed for induction machine using audible noise recorded by a hand-held smartphone in (Vaimann *et al.*, 2018), and different faults are investigated, then, the results are compared with the results of mechanical vibrations measurements.

However, according to our assessment of the literature, no research has been done to detect the fault of rotating diode rectifier in the brushless synchronous generator using the analysis of sound signals. In this paper, due to impossibility of direct access to the rectifier bridge in the brushless synchronous generator, a fault detection method is proposed based on the recorded acoustic signals of the generator in which there is no necessity of direct access to the rectifier. In addition, multiple conditions such as different mother wavelet and decomposition level and different distance functions are compared to provide the enhanced fault detection. The proposed method is tested on a brushless synchronous generator in the laboratory under no-load and full-load conditions. The proposed method is based on a signal processing method and could be applied to other signals like vibration, stray flux, voltage, and current. However, due to the mentioned advantage of acoustic signals for fault detection, it is considered

for fault detection here. The proposed method is devised for a diode open-circuit and a phase open-circuit fault detection in the brushless synchronous generator but it is not limited to these faults and can be used for detection of other electrical faults such as stator winding internal faults, short circuit fault, and bar breaking fault in the rotor. Beside electrical faults, it could be also utilised for a mechanical fault like bearing or eccentricity faults.

This article is structured as follows. In the next section general information about synchronous generator is provided and the structure of a brushless synchronous generator is presented. Then, the wavelet transform is studied in which the relative energy of a decomposed signal by wavelet is formulated. After that, the KNN method is discussed and different distance functions and distance weights for the method are introduced. In the test rig section, to evaluate the proposed classification method for the rectifier bridge of brushless synchronous generator fault detection, the experimental results are used and classified by different states which are compared for accuracy. The article ends with the conclusion about the presented work.

2. Brushless synchronous generator

The conversion of mechanical energy into electrical energy in power plants is carried out by generators. Most generators used in power plants are synchronous. Synchronous generators are dual port electrical machine and to produce the voltage and current at the output of the generator, it is necessary to provide the voltage and direct current to the winding of their field. There are several ways to reach this, such as the use of auxiliary DC generator, the use of auxiliary synchronous generator, the use of power electronic converters, each of which has some advantages and disadvantages whose discussion is beyond the scope of this research.

Brushless synchronous generators have been used to increase reliability and reduce the need for maintenance and repair in many of the power plants or sensitive applications, such as submarines or aircrafts. As in the Fig. 1 it can be seen that in this case, the main
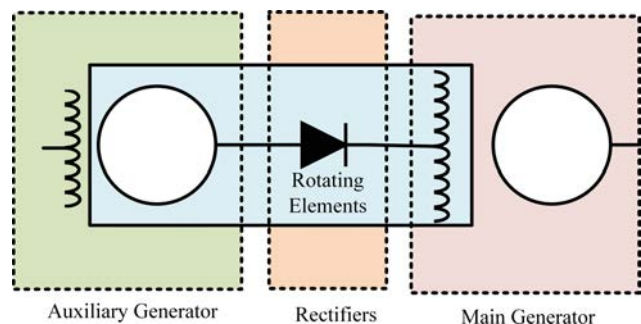

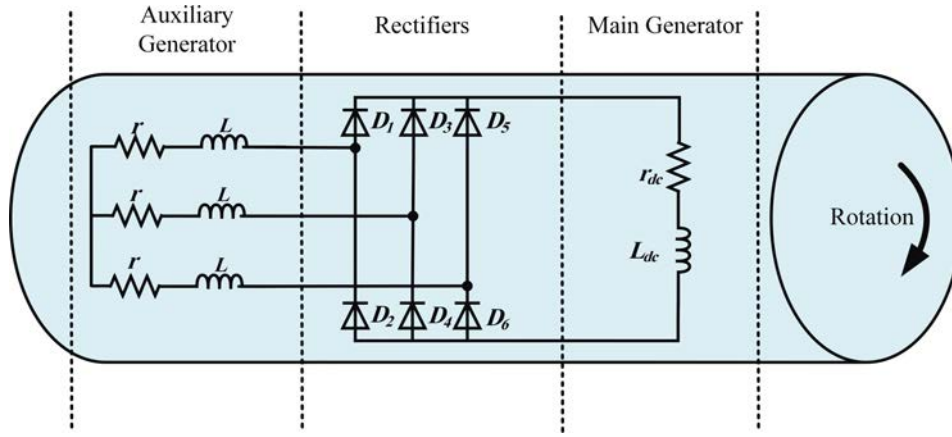Fig. 1. Block diagram of a brushless synchronous generator.

Fig. 2. Electrical rotating components of a brushless synchronous generator.

generator field power supply is provided by another synchronous generator and a rectifier set. Due to the fact that in the synchronous generator, the field winding is located opposite to the main generator on the stator and induced on the rotor coil, this type of synchronous generator is named inverse synchronous generator. The removal of brushes and rings, which are used in other systems to transfer the required power to the main generator field coil, is the advantage of this type of system.

According to Fig. 2, in auxiliary synchronous generator, induced voltage arises on rotor winding and this alternating voltage is rectified by rectifiers mounted on the rotating shaft which is the only source of the main generator field winding. Therefore, monitoring the status of the rectifier is very important.

3. Wavelet transform

Wavelet transform decomposes a signal into different levels of frequency resolution which are called wavelets (KOCAMAN, ÖZDEMIR, 2009). The wavelet family $\psi_{a,b}$ is obtained from a unique mother (prototype) wavelet $\psi(t)$ which is dilated by factor a and transformed by factor b as

$$\psi_{a,b} = \frac{1}{\sqrt{a}} \psi\left(\frac{t-b}{a}\right), \qquad (1)$$

where a and b take values in $\mathfrak{R}$, and t is time (SHENSA, 1992). The wavelet transform is often discretised in a and b by special values of discrete sets of factors, $a_j = 2^j$ and $b_{j,k} = 2^j k$. Actually, j is a scale factor and k is a shift factor. Therefore, the family becomes

$$\psi_{j,k} = 2^{-j/2} \psi\left(2^{-j}t - k\right), \qquad (2)$$

where $\psi_{j,k}$ is for an orthonormal basis of square integrable space $L^2(\mathfrak{R})$ (AKIN, 2002; GUO *et al.*, 2009). Therefore, the wavelet discrete transform of $f(t)$ is as

$$W(j,k) = 2^{-j/2} \int \psi\left(2^{-j}t - k\right) f(t)\,\mathrm{d}t. \qquad (3)$$

In the above equation j stands for time and k is the frequency. The Eq. (3) is discretised to be applicable for discrete signals as

$$w(j,k) = 2^{-j/2} \sum_i \psi\left(2^{-j}i - k\right) f(i). \qquad (4)$$

Figure 3 is an illustration of level-4 decomposition of the discrete signal F. $A_1, ..., A_4$ represent an approximation of F, and $D_1, ..., D_4$ are the representatives of the local details. In order to make the wavelet useful for signal classification, the concept of relative wavelet energy can be applied which provides information at different frequency bands. For a level-N decomposition, the energy at each decomposition is as Eq. (5) (GUO *et al.*, 2009). The energy of A_N is E_{A_N} and is defined as Eq. (6)

$$E_{D_j} = \sum_k |D_j[k]|^2, \qquad j = 1, ..., N, \qquad (5)$$
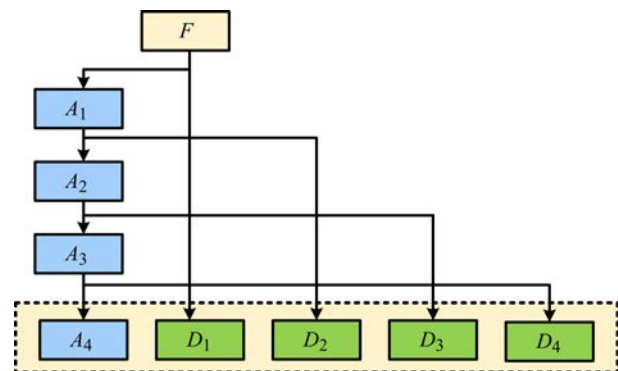
$$E_{A_N} = \sum_k |A_N[k]|^2. \qquad (6)$$

Fig. 3. Level-4 decomposition of discrete signal F.

The total energy of the decomposed signal is

$$E_{\text{tot}} = E_{A_N} + \sum_{j=1}^{N} E_{D_j}. \qquad (7)$$

Therefore, the relative wavelet energy of each decomposition is defined as

$$\rho_{(D_j \text{ or } A_N)} = \frac{E_{(D_j \text{ or } A_N)}}{E_{\text{tot}}} \times 100, \tag{8}$$

where

$$\rho_{A_N} + \sum_{j=1}^{N} \rho_{D_j} = 100. $$

4. K-Nearest Neighbours

KNN is a classification method in which an object is classified by its distance to the k neighbours. Indeed, for a given set of n pairs $(\mathbf{x}_1, y_1), ..., (\mathbf{x}_n, y_n)$ in which $\mathbf{x}_i$, the input vector, and y_i, the class label of $\mathbf{x}_i$, take values in the sets $\mathfrak{R}^d$ and $\{1, 2, ..., M\}$, respectively, for each $\mathbf{x}_i$, k target neighbours are specified with the same labels that are desired for being nearest to $\mathbf{x}_i$ (Cover, Hart, 1967; Short, Fukunaga, 1981). When $k = 1$, it means that $\mathbf{x}_i$ will be assigned to a nearest class. Therefore, in KNN method two parameters play significant role in classification accuracy, and these are k and the distance calculation function. According to (Cover, Hart, 1967), among all KNN rules, the single nearest rule ($k = 1$) is appropriate. On the other hand, there are several distance function methods including Minkowski metric (Eq. (9)), Euclidean distance (Eq. (10)), Standardised Euclidean distance (Eq. (11)), Mahalanobis distance (Eq. (12)), City block metric (Eq. (13)), Chebychev distance (Eq. (14)), Cosine distance (Eq. (15)), Correlation distance (Eq. (16)), and some other functions. The distance between the vector $\mathbf{x}_t$ and $\mathbf{x}_s$ for an m-by-n input data matrix $\mathbf{X}$ by each distance metric is defined as follows:

$$\mathbf{d}_{st} = \sqrt[p]{\sum_{j=1}^{n} |\mathbf{x}_{sj} - \mathbf{x}_{tj}|}, \tag{9}$$

$$\mathbf{d}_{st}^2 = (\mathbf{x}_s - \mathbf{x}_t)(\mathbf{x}_s - \mathbf{x}_t)^{\mathrm{T}}, \tag{10}$$

$$\mathbf{d}_{st}^2 = (\mathbf{x}_s - \mathbf{x}_t)\mathbf{V}^{-1}(\mathbf{x}_s - \mathbf{x}_t)^{\mathrm{T}}, \tag{11}$$

$$\mathbf{d}_{st}^2 = (\mathbf{x}_s - \mathbf{x}_t)\mathbf{C}^{-1}(\mathbf{x}_s - \mathbf{x}_t)^{\mathrm{T}}, \tag{12}$$

$$\mathbf{d}_{st} = \sum_{j=1}^{n} |\mathbf{x}_{sj} - \mathbf{x}_{tj}|, \tag{13}$$

$$\mathbf{d}_{st} = \max\{|\mathbf{x}_{sj} - \mathbf{x}_{tj}|\}, \tag{14}$$

$$d_{st} = \left(1 - \frac{\mathbf{x}_s \mathbf{x}_t^{\mathrm{T}}}{\sqrt{(\mathbf{x}_s \mathbf{x}_s^{\mathrm{T}})(\mathbf{x}_t \mathbf{x}_t^{\mathrm{T}})}}\right), \tag{15}$$

$$d_{st} = 1 - z^*, \tag{16}$$

where

$$z^* = \frac{(\mathbf{x}_s - \overline{x}_s)(\mathbf{x}_t - \overline{x}_t)}{\sqrt{[(\mathbf{x}_s - \overline{x}_s)(\mathbf{x}_s - \overline{x}_s)^{\mathrm{T}}][(\mathbf{x}_t - \overline{x}_t)(\mathbf{x}_t - \overline{x}_t)^{\mathrm{T}}]}}$$

and in Eq. (11) $\mathbf{V}$ is the n-by-n diagonal matrix in which each diagonal element is square of the vector containing the inverse weights; in Eq. (12) $\mathbf{C}$ is the covariance matrix; and in Eq. (16) $\overline{x}_s$ and $\overline{x}_t$ is obtained by Eqs (17) and (18), respectively.

$$\overline{x}_s = \frac{1}{n}\sum_j \mathbf{x}_{sj}, \tag{17}$$

$$\overline{x}_t = \frac{1}{n}\sum_j \mathbf{x}_{tj}. \tag{18}$$

According to Eqs (9), (11), (13), and (14), for the special cases of p in Minkowski metric some other metrics are derived including city block metric for $p = 1$, Euclidean distance for $p = 2$, and Chebychev distance for $p = \infty$.

In order to evaluate the classification, v-fold cross-validation can be used. In v-fold cross-validation, the original data are partitioned into v equal size subsets randomly. Of v subsets, v-1 subsets are used for training and one subset is used for evaluation. The classifier error is then obtained by fraction of misclassified observations. Besides, the classifier accuracy is defined as fraction of accurately classified observations to all observations.

5. Investigated fault classes

Since there is no mechanical wear between rotating components for power transmission to generator field windings in brushless synchronous generators, there is less need for maintenance than when using other methods which require brushes and rings. Due to the fact that the rectifiers are rotating with other electrical components and there is no direct access to them, the diode is usually used for rectifying.

Some of the causes that can lead to diode faults include rise in temperature, load increase, and transient voltages. One of the most likely faults occurring during a run is the diode open-circuit. As shown in Fig. 4a, one of the rectifier diode is open-circuited. Given that the supply of rectifier bridge is symmetrical, the effect of the open-circuiting another diode will be similar. This fault is one of the evaluated fault states.

In the fault case of one diode open-circuit, if another open-circuit fault occurs on the diode in the same leg of rectifier, a new category of fault is defined. As seen in Fig. 4b, the occurrence of this fault is similar to the one phase open-circuiting of the rectifier bridge feeder.
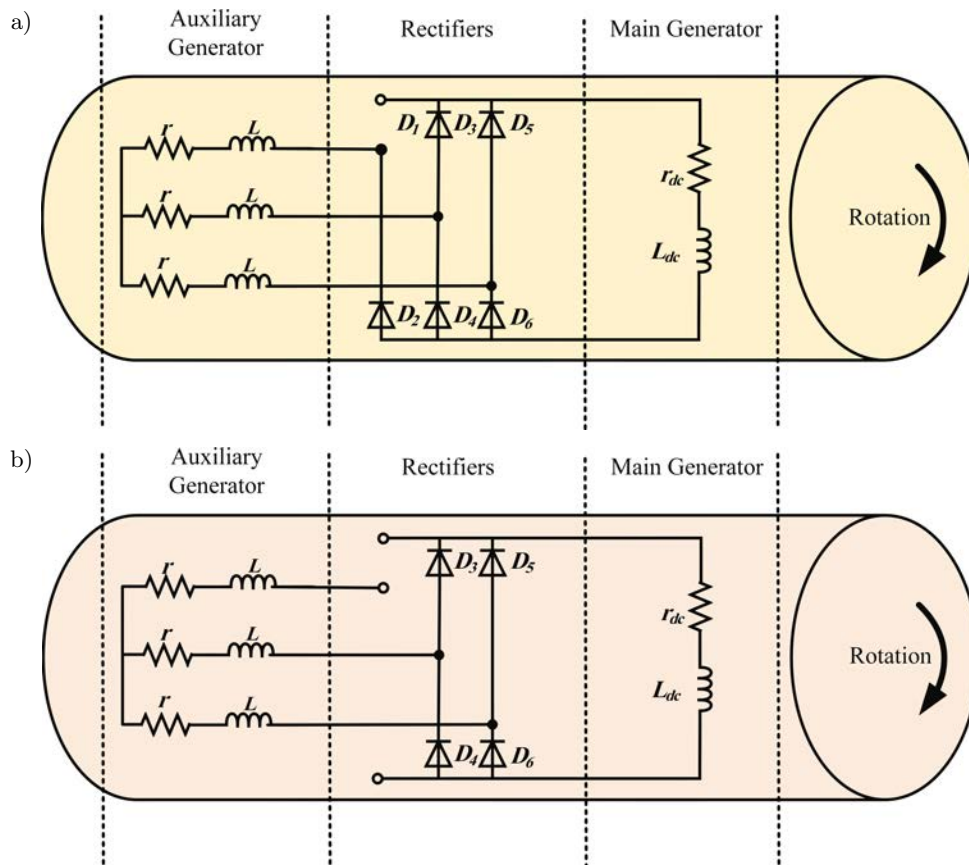
Fig. 4. Investigated open-circuit faults: a) one diode open-circuit and b) two diode open-circuit, of rotary rectifier along with other electrical rotating components.

6. Proposed fault detection method

In order to classify the normal and faulty conditions of the field rectifier bridge of a generator, the sound signal of the machine is recorded in different case study states for learning the classifier. The wavelet transform of the recorded signal is derived using wavelet functions Coif-4 (Coiflets), Sym-6 (Symlets), and db-6 (Daubechies) and for different decomposition levels. Then, the relative energy of the transformed signal is calculated and utilising KNN classification method, in this step for finding the best mother wavelet and decomposition level, distance function is considered Euclidean distance and the effect of distance of neighbors are the same (equal). The classification accuracy is calculated for each wavelet function and decomposition level. The mother wavelet and decomposition level by which the maximum accuracy is achieved is chosen for the next steps. Next, using distance functions, Minkowski metric, Euclidean distance, Standardised Euclidean distance, Mahalanobis distance, City block metric, Chebychev distance, Cosine distance, and Correlation distance and distance weights, Equal, Inverse, and Squared inverse the classification accuracy is calculated. The maximum classification accuracy is considered by the distance function and weight as the best

classifier state for the rectifier bridge fault detection using acoustic signals.
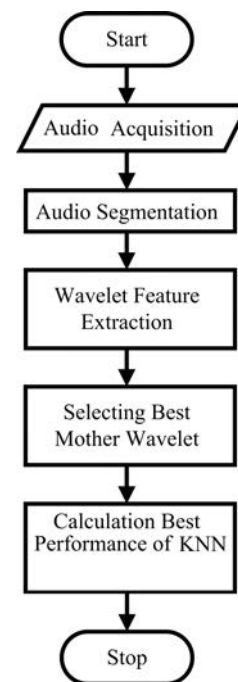

Fig. 5. Flowchart of the rectifier faults classification.

7. Test rig

To evaluate the proposed fault detection method, a three phase 380 V, 11 kVA, 4 poles brushless synchronous generator has been used. It is necessary to create faulty conditions that would have access to rotating diodes. As is shown in Fig. 6, some modifications are performed. First of all, the shaft of the generator is expanded and five rings are installed on it: three rings for bringing out the output of the auxiliary generator and two rings for entering rectified voltage to the field winding of the main generator. Then modifications have been made in the circuit of the three-phase diode rectifier and six switches are added that can easily open circuit each diode.
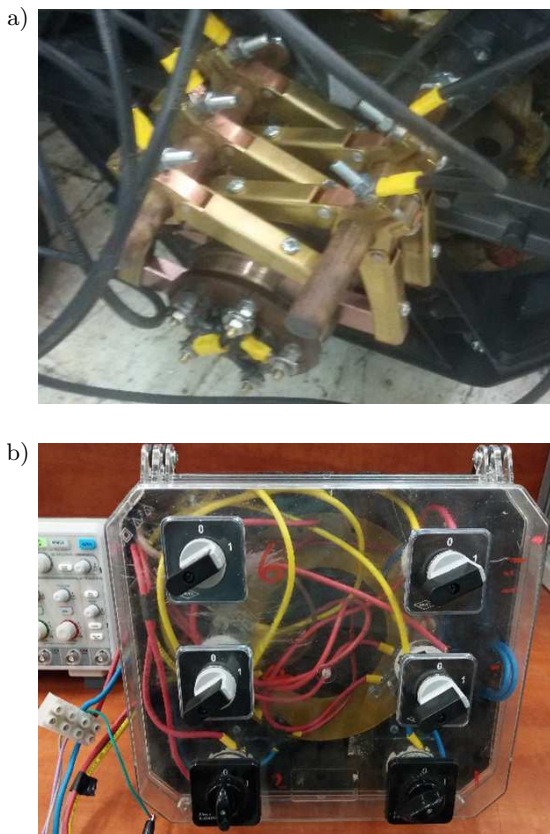

Fig. 6. Modification on brushless synchronous generator to simulate faulty conditions: a) brushes and rings, b) rectifier bridge with switches.

An experimental set has been installed according to Figs 7 and 8. The set comprises a modified brushless synchronous generator, the three phase induction motor for driving the generator, the switch set for applying faults, the DC supply for feeding field winding of auxiliary generator, the microphone set for recording the sound, the three-phase electric load and the electrical drive for rotating motor and generator at synchronous speed.

Electrical and mechanical connections and measuring system diagram for elements of the experimental
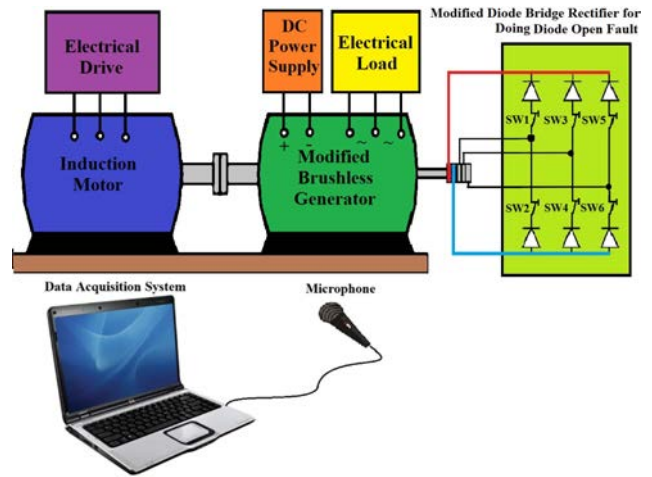

Fig. 7. Connection diagram for electrical and mechanical elements and measuring system.
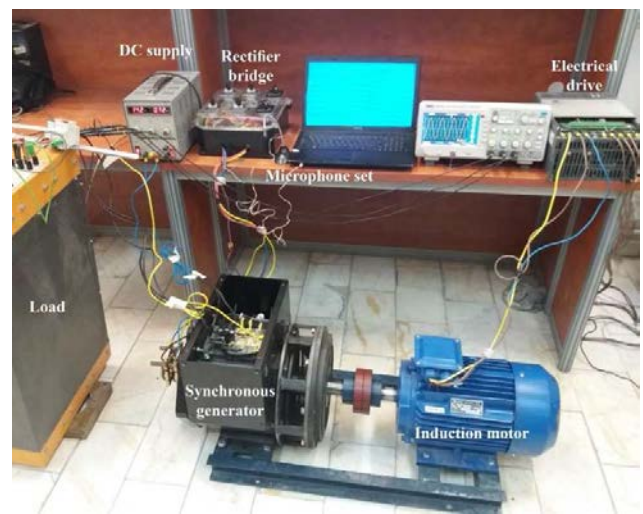

Fig. 8. Laboratory set.

set are shown in Fig. 7. The discussed faults on the diode rectifier bridge are one diode open-circuit fault and one phase loss could be reached by turning off any of the switches from one to six for diode open-circuit fault and turning off the switches one and two, or three and four, or five and six leads to one phase loss.

Figure 9 illustrates the sound signals for six states including two normal conditions and four faulty ones. The recorded sound is then divided into ten equal time one second interval samples for each of the six states. The sound recording sample rate is 48000 Hz and the sixty discrete samples are transformed by the mother wavelet. The wavelet function is chosen to be Coif-4 (Coiflets), Sym-6 (Symlets), and db-6 (Daubechies), and decomposition level is chosen to be up to level-5. Then, the relative wavelet energy of each fault state of the rectifier by the mentioned cases is calculated. The results of the mentioned procedure implemented for relative energy of all states for 4 level decomposition using sym mother wavelet are presented in Tables 1–6.
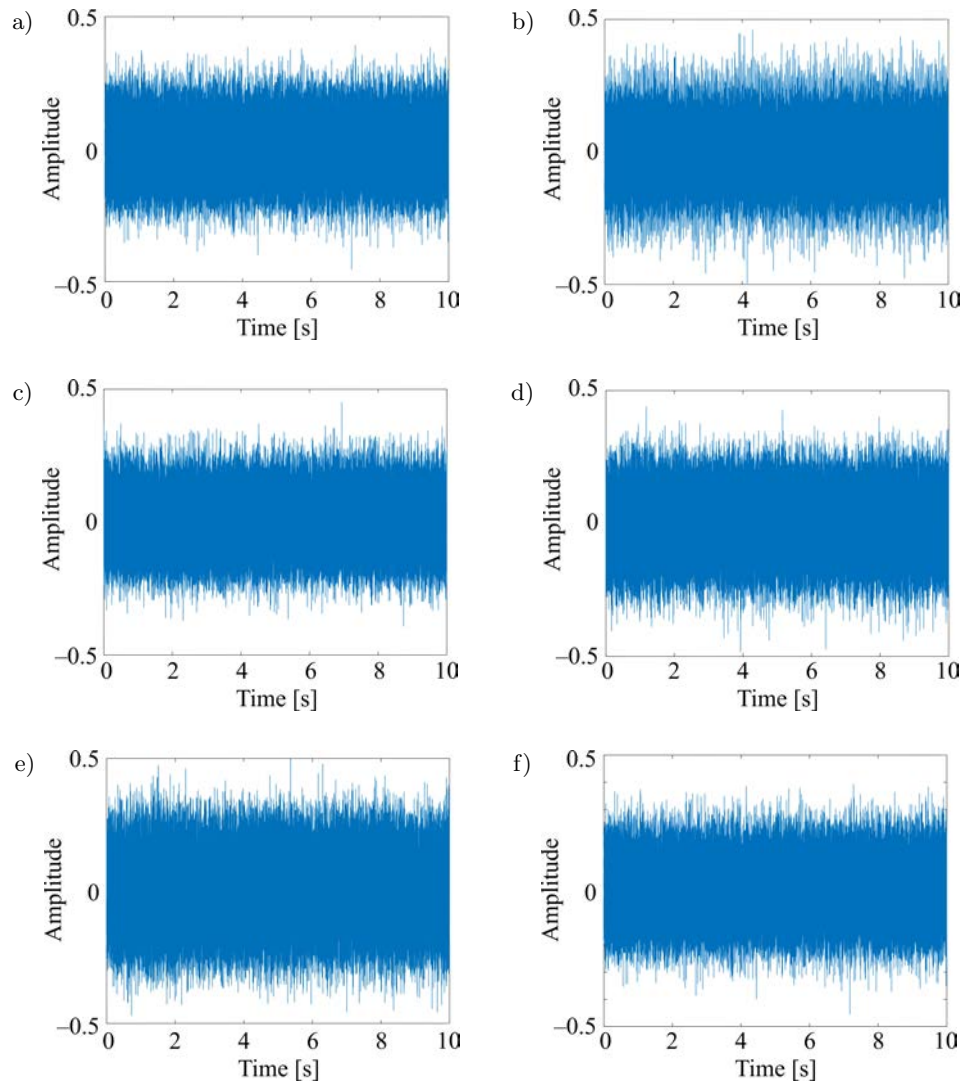
Fig. 9. Sound signals for six states: a) normal, no-load; b) normal, full-load; c) one diode open-circuit, no-load; d) one diode open-circuit, full-load; e) two diode open-circuit, no-load; f) two diode open-circuit, full-load.

Table 1. The relative energy of level-4 wavelet decomposition for ten 1-second sound samples of normal and no-load state.

ρ_{A4}	ρ_{D1}	ρ_{D2}	ρ_{D3}	ρ_{D4}
88.989	0.066	1.184	2.563	7.198
88.417	0.063	1.284	2.949	7.287
88.187	0.069	1.430	3.050	7.264
89.609	0.062	1.227	2.767	6.335
88.585	0.067	1.336	2.940	7.072
89.240	0.064	1.211	2.789	6.697
89.169	0.064	1.350	2.875	6.543
88.922	0.063	1.297	2.903	6.815
88.544	0.061	1.286	2.904	7.205
88.727	0.060	1.300	2.855	7.058

Table 2. The relative energy of level-4 wavelet decomposition for ten 1-second sound samples of normal and full-load state.

ρ_{A4}	ρ_{D1}	ρ_{D2}	ρ_{D3}	ρ_{D4}
70.674	0.175	8.872	14.562	5.718
68.784	0.160	9.181	15.118	6.756
70.758	0.163	8.895	14.232	5.953
70.467	0.174	9.372	14.427	5.560
71.159	0.173	8.281	13.794	6.593
71.819	0.150	8.364	13.529	6.138
69.755	0.167	9.329	14.720	6.029
71.707	0.168	8.680	13.162	6.283
69.833	0.151	9.037	14.299	6.681
71.338	0.153	8.450	14.235	5.824

Table 3. The relative energy of level-4 wavelet decomposition for ten 1-second sound samples of one diode open-circuit and no-load state.

ρ_{A4}	ρ_{D1}	ρ_{D2}	ρ_{D3}	ρ_{D4}
92.008	0.059	1.013	2.107	4.813
92.596	0.049	0.928	1.983	4.444
91.984	0.056	1.071	2.291	4.598
91.852	0.055	1.076	2.180	4.837
92.239	0.047	0.967	2.067	4.680
92.116	0.051	0.958	2.026	4.848
92.129	0.051	0.929	2.087	4.804
92.423	0.049	0.875	1.967	4.686
92.672	0.051	0.912	1.996	4.370
92.305	0.052	0.943	1.959	4.741

Table 4. The relative energy of level-4 wavelet decomposition for ten 1-second sound samples of one diode open-circuit and full-load state.

ρ_{A4}	ρ_{D1}	ρ_{D2}	ρ_{D3}	ρ_{D4}
78.298	0.143	7.664	9.154	4.741
78.510	0.143	7.400	9.277	4.670
76.082	0.141	8.689	10.043	5.044
77.756	0.138	7.885	9.220	5.002
78.862	0.127	7.551	8.830	4.629
78.115	0.132	7.289	9.801	4.664
75.937	0.146	8.454	10.571	4.892
78.079	0.123	7.193	9.808	4.797
77.800	0.130	7.761	9.678	4.630
75.070	0.140	8.481	10.759	5.550

Table 5. The relative energy of level-4 wavelet decomposition for ten 1-second sound samples of two diode open-circuit and no-load state.

ρ_{A4}	ρ_{D1}	ρ_{D2}	ρ_{D3}	ρ_{D4}
90.091	0.073	1.124	2.576	6.136
89.793	0.077	1.194	2.815	6.122
89.841	0.067	1.138	2.722	6.232
89.645	0.070	1.232	2.945	6.107
89.543	0.074	1.253	2.893	6.236
89.749	0.066	1.161	2.889	6.135
89.577	0.063	1.126	2.817	6.418
90.198	0.066	1.176	2.773	5.786
89.933	0.070	1.238	3.019	5.740
89.503	0.073	1.263	2.924	6.236

The calculated relative energy of the wavelet is used for classification by KNN technique (distance function

Table 6. The relative energy of level-4 wavelet decomposition for ten 1-second sound samples of two diode open-circuit and full-load state.

ρ_{A4}	ρ_{D1}	ρ_{D2}	ρ_{D3}	ρ_{D4}
72.504	0.145	9.082	12.196	6.073
71.494	0.146	9.204	12.908	6.249
72.121	0.148	9.014	11.843	6.875
71.313	0.140	9.316	12.813	6.418
72.422	0.135	8.828	12.238	6.377
72.681	0.153	9.136	11.801	6.229
72.726	0.160	8.898	11.685	6.531
72.267	0.176	8.950	12.247	6.360
70.498	0.195	9.154	13.047	7.106
71.326	0.156	9.175	12.873	6.470

of Euclidean distance and distance weight of equal). In order to find the best mother wavelet and decomposition level, the classification accuracy with respect to decomposition level is shown in Fig. 10 for the three mentioned wavelet functions. According to the figures, for all three wavelet functions, level-4 decomposition leads to better accuracy. In addition, by Sym-6 wavelet function the classification accuracy results in about 97.1, which is the highest value among these cases.

The other parameters which affect the classification accuracy are distance function and distance weight. By choosing Sym-6 level-4 decomposition of the wavelet transformation, the distance function and distance weight of KNN classification are changed and the results of classification accuracy are presented in Table 7. According to the table, the best accuracy is achieved by the distance weight of inverse and the distance function of Euclidean, Chebychev, Cosine, and Minkowski.

Table 7. Classification accuracy for different distance function and distance weight of KNN.

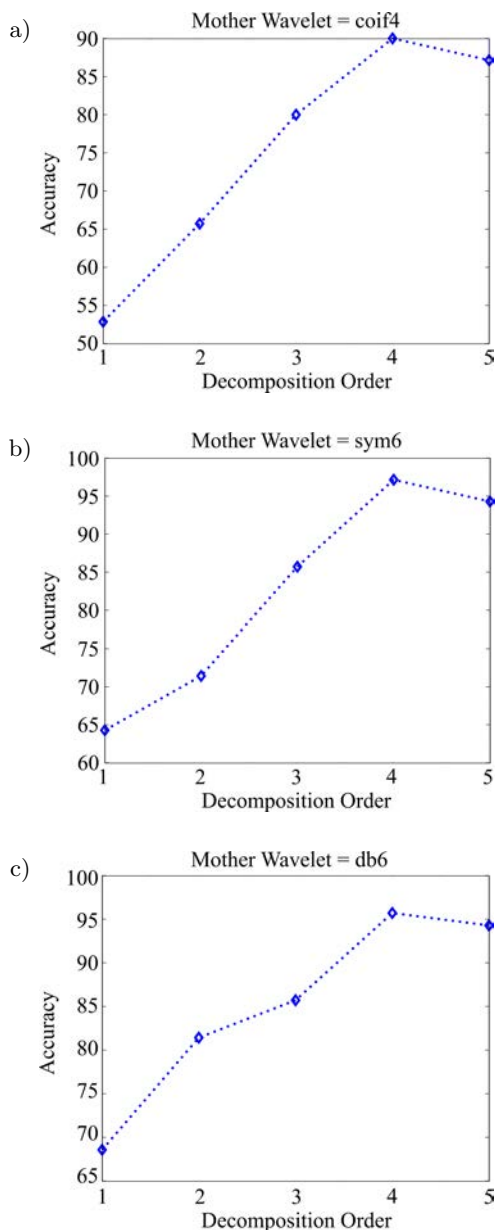| Distance function	Distance weight		
	Equal	Inverse	Squared inverse
Euclidean	97.15	98.57	97.14
Cityblock	97.15	97.14	95.71
Chebychev	97.15	98.57	95.71
Correlation	95.71	94.29	95.71
Cosine	95.71	98.57	97.14
Mahalanobis	95.71	95.71	94.29
Minkowski	97.14	98.57	97.14
Standardized Euclidean	88.57	91.42	90.00

a)

b)

c)

Fig. 10. Classification accuracy with respect to decomposition level by wavelet functions: a) Coif-4; b) Sym-6; c) db-6.

8. Conclusion and future work

In this paper, fault detection and classification method of the rotary rectifier of brushless synchronous generators have been investigated. The considered fault classes are one diode open-circuit and two diodes open-circuited which lead to the opening of one armature phase of the auxiliary generator. Since there is no need to destruct the structure of the machine in fault diagnosis using the sound signal, this method has been suggested for fault detection. Therefore, sound signals are recorded for a healthy situation of the machine and two modes of fault are recorded under no load and full-load conditions of the main generator. Characteristic

extraction is performed using the wavelet transform and the classification is carried out by KNN method.

To select the suitable mother wavelet and the decomposition level of the main signal, a comparison was made between the db-6, Coif-4, and Sym-6 wavelets. The best performance is achieved by the level-4 decomposition of the main signal by sym wavelet. In addition, in the KNN method different distance functions and distance weights are compared for selecting the best accuracy of classification. The Euclidean, Chebychev, Cosine, Minkowski distance functions in Inverse distance weight had the best accuracy performance.

For future work, short-circuit fault happening on the rotating diode and discrimination between short circuited and open circuited fault are suggested. For implementing this idea, time, frequency, and time-frequency domains need to be investigated. Due to the importance of reducing the repair time in the big brushless generator, finding the location of the faulty diode should also be considered.

References

1. AKIN M. (2002), *Comparison of wavelet transform and FFT methods in the analysis of EEG signals*, Journal of Medical Systems, **26**, 3, 241–247, doi: 10.1023/A:1015075101937.

2. COVER T., HART P. (1967), *Nearest neighbor pattern classification*, IEEE Transactions on Information Theory, **13**, 1, 21–27, doi: 10.1109/TIT.1967.1053964.

3. CHACON J.L.F., KAPPATOS V., BALACHANDRAN W., GAN T.H. (2015), *A novel approach for incipient defect detection in rolling bearings using acoustic emission technique*, Applied Acoustics, **89**, 88–100, doi: 10.1016/j.apacoust.2014.09.002.

4. GLOWACZ A. (2015), *Recognition of acoustic signals of loaded synchronous motor using FFT, MSAF-5 and LSVM*, Archives of Acoustics, **40**, 2, 197–203, doi: 10.1515/aoa-2015-0022.

5. GLOWACZ A. (2016), *Fault diagnostics of acoustic signals of loaded synchronous motor using SMOFS-25-EXPANDED and selected classifiers*, Tehnicki vjesnik – Technical Gazette, **23**, 5, 1365–1372, doi: 10.17559/TV-20150328135652.

6. GLOWACZ A. (2018), *Acoustic-based fault diagnosis of commutator motor*, Electronics, **7**, 11, 299, doi: 10.3390/electronics7110299.

7. GLOWACZ A., GLOWACZ W., GLOWACZ Z., KOZIK J. (2018), *Early fault diagnosis of bearing and stator faults of the single-phase induction motor using acoustic signals*, Measurement, **113**, 1–9, doi: 10.1016/j.measurement.2017.08.036.

8. GLOWACZ A., GLOWACZ Z. (2017a), Diagnosis of stator faults of the single-phase induction motor using acoustic signals, *Applied Acoustics*. Elsevier, **117**, 20–27, doi: 10.1016/j.apacoust.2016.10.012.

9. GLOWACZ A., GLOWACZ Z. (2017b), *Recognition of rotor damages in a DC motor using acoustic signals*, Bulletin of the Polish Academy of Sciences: Technical Sciences, **65**, 2, 187–194, doi: 10.1515/bpasts-2017-0023.

10. GUO L., RIVERO D., SEOANE J.A., PAZOS A. (2009), *Classification of EEG signals using relative wavelet energy and artificial neural networks*, [in:] Proceedings of the first ACM/SIGEVO Summit on Genetic and Evolutionary Computation – GEC '09, New York, New York, USA: ACM Press, pp. 177–184, doi: 10.1145/1543834.1543860.

11. HAROUN S., SEGHIR A.N., TOUATI S. (2018), *Multiple features extraction and selection for detection and classification of stator winding faults*, IET Electric Power Applications, **12**, 3, 339–346, doi: 10.1049/iet-epa.2017.0457.

12. HU C.Z., YANG Q., HUANG M.Y., YAN W.J. (2017), *Sparse component analysis-based under-determined blind source separation for bearing fault feature extraction in wind turbine gearbox*, IET Renewable Power Generation, **11**, 3, 330–337, doi: 10.1049/iet-rpg.2016.0240.

13. KOCAMAN Ç., ÖZDEMIR M. (2009), *Comparison of statistical methods and wavelet energy coefficients for determining two common PQ disturbances: Sag and swell*, [in:] Electrical and Electronics Engineering, 2009. ELECO 2009. International Conference on, pp. I-80–I-84, doi: 10.1109/ELECO.2009.5355235.

14. Narendiranath Babu T. *et al.* (2018), *Application of EMD, ANN and DNN for self-aligning bearing fault diagnosis*, Archives of Acoustics, **43**, 2, 163–175, doi: 10.24425/aoa.2018.125166.

15. PRAVEENKUMAR T., SABHRISH B., SAIMURUGAN M., RAMACHANDRAN K.I. (2018), *Pattern recognition based on-line vibration monitoring system for fault diagnosis of automobile gearbox*, Measurement, **114**, 233–242, doi: 10.1016/j.measurement.2017.09.041.

16. REZAZADEH MEHRJOU M., MARIUN N., MISRON N., RADZI M., MUSA S. (2017), *Broken rotor bar detection in LS-PMSM based on startup current analysis using wavelet entropy features*, Applied Sciences, **7**, 8, 845, doi: 10.3390/app7080845.

17. SHAH A.M., BHALJA B.R. (2016), *Fault discrimination scheme for power transformer using random forest technique*, IET Generation, Transmission & Distribution, **10**, 6, 1431–1439, doi: 10.1049/iet-gtd.2015.0955.

18. SHENSA M.J. (1992), *The discrete wavelet transform: wedding the a trous and Mallat algorithms*, IEEE Transactions on Signal Processing, **40**, 10, 2464–2482, doi: 10.1109/78.157290.

19. SHORT R., FUKUNAGA K. (1981), *The optimal distance measure for nearest neighbor classification*, IEEE Transactions on Information Theory, **27**, 5, 622–627, doi: 10.1109/TIT.1981.1056403.

20. SINGH A., PAREY A. (2017), *Gearbox fault diagnosis under fluctuating load conditions with independent angular re-sampling technique, continuous wavelet transform and multilayer perceptron neural network*, IET Science, Measurement & Technology, **11**, 2, 220–225, doi: 10.1049/iet-smt.2016.0291.

21. VAIMANN T., SOBRA J., BELAHCEN A., RASSÕLKIN A., ROLAK M., KALLASTE A. (2018), *Induction machine fault detection using smartphone recorded audible noise*, IET Science, Measurement & Technology, **12**, 4, 554–560, doi: 10.1049/iet-smt.2017.0104.

22. WANG L.-H., ZHAO X.P., WU J.X., XIE Y.Y., ZHANG Y.H. (2017), *Motor fault diagnosis based on short-time Fourier transform and convolutional neural network*, Chinese Journal of Mechanical Engineering, **30**, 6, 1357–1368, doi: 10.1007/s10033-017-0190-5.

23. ZHANG C., PENG Z., CHEN S., LI Z., WANG J. (2018), *A gearbox fault diagnosis method based on frequency-modulated empirical mode decomposition and support vector machine*, Proceedings of the Institution of Mechanical Engineers, Part C: Journal of Mechanical Engineering Science, **232**, 2, 369–380, doi: 10.1177/0954406216677102.